

# Morphological Tuning of Polymeric Nanoparticles via Microfluidic Platform for Fuel Cell Applications

Mohammad Mahdi Hasani-Sadrabadi,<sup>\*,†,‡,§</sup> Fatemeh Sadat Majedi,<sup>†,‡</sup> Jules John VanDersarl,<sup>†</sup> Erfan Dashtimoghdam,<sup>§</sup> S. Reza Ghaffarian,<sup>§</sup> Arnaud Bertsch,<sup>†</sup> Homayoun Moaddel,<sup>||</sup> and Philippe Renaud<sup>\*,†</sup>

<sup>†</sup>Laboratoire de Microsystemes (LMIS4), Institute of Microengineering and <sup>‡</sup>Institute of Bioengineering, École Polytechnique Fédérale de Lausanne (EPFL), CH-1015 Lausanne, Switzerland

<sup>§</sup>Department of Polymer Engineering and Color Technology, Amirkabir University of Technology, Tehran, Iran

<sup>||</sup>Hydrogen & Fuel Cell Inc., Arcadia, California 91006, United States

## S Supporting Information

**ABSTRACT:** At nanoscale length scales, the properties of particles change rapidly with the slightest change in dimension. The use of a microfluidic platform enables precise control of sub-100 nm organic nanoparticles (NPs) based on polybenzimidazole. Using hydrodynamic flow focusing, we can control the size and shape of the NPs, which in turn controls a number of particle material properties. The anhydrous proton-conducting nature of the prepared NPs allowed us to make a high-performance ion exchange membrane for fuel cell applications, and microfluidic tuning of the NPs allowed us subsequently to tune the fuel cell performance.

Particles with nanoscale dimensions have long been known to have properties distinct from their bulk counterparts.<sup>1</sup> This opportunity to alter and tune material properties has made nanoparticles (NPs) a popular research area across a range of scientific disciplines. Polymeric NPs can be synthesized using either top-down or bottom-up processing. As bottom-up processing involves the self-assembly of particles via intermolecular forces, it offers the greatest opportunities to tailor the particle structure and properties.<sup>2</sup> However, this is both a powerful and unruly technique, as it comes with the price of being much more challenging to control.<sup>3</sup>

The NP synthesis technique influences the particle parameters and therefore plays the main role in determining the potency of the NPs; ideally, it should produce reproducible, stable, and homogeneous particles.<sup>3</sup> In NP synthesis, the particle size and the size distribution are of great importance. Considering this, engineers often choose the robust antisolvent precipitation technique.<sup>4</sup> Since this technique is based on solvent displacement and subsequent polymer precipitation, the diffusion time at the solvent–nonsolvent interface mainly determines the particle size. For amphiphatic polymers, the time of aggregation ( $\tau_{\text{agg}}$ ) also strongly affects the particle size.<sup>5</sup> Because  $\tau_{\text{agg}}$  is an intrinsic material property, it cannot be adjusted through microfluidic manipulation. However, the *effective* time of aggregation can be shortened by having the time of mixing ( $\tau_{\text{mix}}$ ) be less than  $\tau_{\text{agg}}$ .<sup>6</sup> Therefore, precise control is required for the diffusion and aggregation process,

but this is very difficult to obtain in bulk syntheses.<sup>7</sup> Microfluidics is an excellent solution to this problem, offering ease of use and control over important variables such as the mixing time. With fine control over a wide range of mixing parameters, microfluidics offers unparalleled control of the reaction process, creating an output of smaller and more monodisperse particles<sup>4</sup> while using very small amounts of valuable reagents.<sup>8,9</sup>

Nafion-based fuel cells traditionally require complex humidification and low-temperature conditions to operate. On the other hand, polybenzimidazole (PBI) is among the most compatible polymers for high-temperature, low-humidity operating conditions in proton exchange membrane fuel cells (PEMFCs).<sup>10</sup> Because of this, scientists have studied composite fuel cell membranes consisting of Nafion and PBI in an effort to capture the best properties of both materials.<sup>11–14</sup> However, maximizing the performance of these composite membranes likely requires precise control of the composite structure, which has not been achieved until the present work. To optimize the properties of the composite membrane, we used microfluidics to synthesize PBI NPs in a range of sizes and shapes and then combined them with Nafion. Finally, we investigated the correlation between the PBI NP morphology and their performance in our composite membrane system.

To control PBI NP precipitation, we used a T-shaped microfluidic device with three inlets and one outlet, which creates hydrodynamic focusing in the main microchip channel (Figure 1a). To ensure stable mixing solely by interfacial diffusion between the water and polymer flows, maintaining stability of the flow in the microchannel is of utmost importance. We used fluorescein sodium (1 mg mL<sup>-1</sup> aqueous solution) as a PBI mimic to demonstrate the focusing ability of the hydrodynamic flow and to determine the range of stable flow rates in the hydrodynamic focusing region. As shown in Figure 1a(ii), the fluorescein stream (0.5  $\mu\text{L min}^{-1}$ ) was hydrodynamically focused by the water streams (10  $\mu\text{L min}^{-1}$ ). The degree of fluorescein stream focusing was tuned by varying the water flow rate (and therefore the flow ratio) to maintain a stable flow-focusing region. For the NP precipitation experi-

Received: August 14, 2012

Published: November 5, 2012



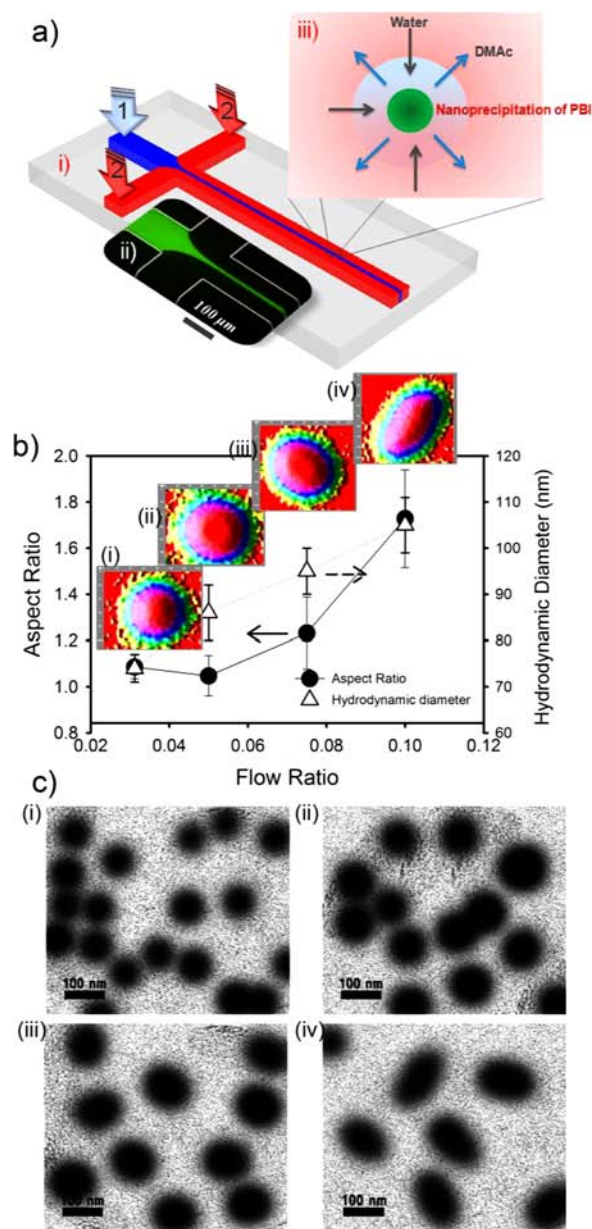


**Figure 1.** (a) (i) Schematic representation of the T-shaped microfluidic device used for hydrodynamic flow focusing of a PBI/DMAc stream using water as a focusing agent. (ii) Image of a fluorescein sodium stream hydrodynamically focused with water (scale bar 100  $\mu\text{m}$ ). (iii) Nanoprecipitation occurs by solvent exchange between water and DMAc at the flow interface. (b) PBI hydrodynamic diameter (based on DLS results) and aspect ratio (based on TEM results and ImageJ analysis) of the fabricated NPs as functions of flow ratio. ImageJ-processed TEM images are also shown as insets. (c) TEM images of PBI NPs synthesized at flow ratios of (i) 0.03, (ii) 0.15, (iii) 0.3, and (iv) 0.1 showing morphological evolution of the NPs from spherical to elliptical (scale bar 100 nm).

ments, the core flow was a PBI solution in *N,N*-dimethylacetamide (DMAc), and the focusing flows were deionized (DI) water [Figure 1a(i)]. Solvent exchange and NP precipitation took place in the main channel at the interface of these two inputs [Figure 1a(iii)].

In this work, we investigated nanoprecipitation of PBI for the first time. PBI is a rodlike polymer that can be rapidly precipitated in the presence of water molecules. The feed

concentration of PBI was 2 mg mL<sup>-1</sup>, and as reported previously, at this concentration PBI chains are in a wormlike conformation.<sup>15</sup> Applied shear forces in the hydrodynamically focused region can transform them into extended wormlike chains, while the presence of water molecules can fix the polymer chains in this state. These characteristics of PBI/DMAc:water systems allowed us to tune the geometry of the prepared NPs as well as their size on the nanoscale (Figure 1c). Moreover, the feed concentration of PBI could be varied to add an additional controlling parameter [see the Supporting Information (SI)].

The interfacial mixing time was controlled by changing the ratio of the water and PBI/DMAc flow rates (in  $\mu\text{L min}^{-1}$ ) from 16:0.5 to 0.75:0.15, resulting in  $\tau_{\text{mix}}$  values ranging from 2.5 to 23 ms (Figure 2 and eq S1 in the SI).

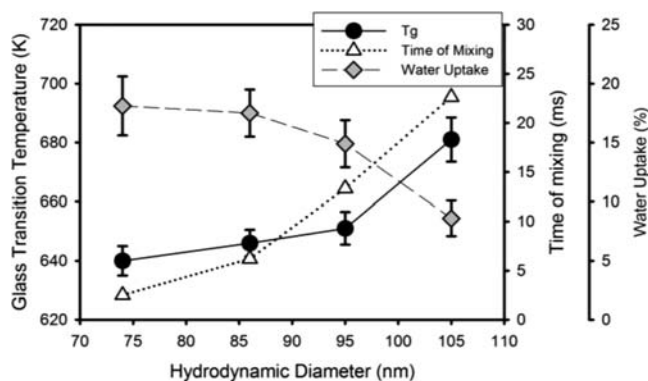


**Figure 2.** Plots of NP water uptake, glass transition temperature ( $T_g$ ), and time of mixing (calculated using eq S1) vs particle size.

Changing the mixing time resulted in a change in particle size. On the basis of dynamic light scattering (DLS) results obtained using the photon correlation spectrometer at Brookhaven, the size of the precipitated NPs increased from  $74 \pm 3$  to  $105 \pm 6$  nm as  $\tau_{\text{mix}}$  increased from 2.5 to 22.6 ms. The size of the particles could continue to increase with increasing  $\tau_{\text{mix}}$  as long as  $\tau_{\text{mix}} < \tau_{\text{agg}}$ . Since the particles grew monotonically over the range of tested mixing times, we can assume that  $\tau_{\text{agg}}$  for the PBI chains is longer than 30 ms. Working in the microfluidic domain where  $\tau_{\text{mix}} < \tau_{\text{agg}}$  leads to NPs that are smaller in size and more homogeneous than the particles prepared by slow (bulk) mixing.<sup>6</sup> Moreover, the particle size distribution (PSD) of PBI NPs prepared using our microfluidic system was  $< 0.2$ , a level of control not possible with bulk synthesis.

High-resolution transmission electron microscopy (HRTEM) images (obtained using a Philips CM200-FEG microscope) of PBI NPs prepared at different flow rates are shown in Figure 1c. ImageJ software was used to examine the PBI NPs, and it was found that the NP aspect ratio ranged from 1 (spherical) to 1.7 (elliptical) (Figure 1b).

Altering the microfluidic time of mixing changed not only the particle size but also the material properties of the NPs. Figure 2 shows the diameter dependence of the glass transition temperature ( $T_g$ ) for PBI NPs obtained using differential scanning calorimetry (DSC). Decreasing the diameter of the PBI NPs decreased  $T_g$  with respect to the  $T_g$  value for bulk PBI, which is  $\sim 698$  K. This trend agrees qualitatively with a previous report for polystyrene NPs.<sup>16</sup> The largest PBI NPs (105 nm) exhibited deviations that can be attributed to the induced

stretching of the polymer that makes the NPs, which gets locked into the extended wormlike state during NP formation. At higher flow ratios, as a result of the increased mixing time, the PBI chains have more time for stretching and transition into the extended wormlike state.

Additionally, water uptake values of the PBI NPs showed a decreasing trend with size. Lower free volumes exist because the PBI chains are more stretched at higher flow ratios. The water uptake also increased as a result of the increased surface area/volume ratio of smaller NPs.

In general, Nafion/PBI blends are formed through membrane casting from DMAc solvent,<sup>17</sup> which is not favorable for ionic phase separation of Nafion.<sup>18</sup> Fortunately, PBI NPs can be dispersed in Nafion-based aqueous solutions. We used a solvent casting technique from aqueous solution, the best known technique for preparation of Nafion-based membranes, to fabricate membranes containing 2.0 wt % PBI NPs.

The effect of the PBI NPs on the physical properties of the Nafion membrane is also important, as strong electrostatic interactions can lead to a reduction in the membrane's free volume. This was confirmed by gas permeability measurements using the constant-pressure/variable-volume method. The room-temperature oxygen/hydrogen permeabilities of pure Nafion and Nafion/PBI-NPs nanocomposite membranes are shown in Figure S9 in the SI. Low fuel permeability, which is highly desirable for PEMFC applications, can be achieved by incorporation of PBI NPs.

The introduction of nonporous NPs with a sufficient level of interaction with the matrix leads to lower gas permeability, an effect enhanced by decreasing the particle size.<sup>19</sup> However, larger NPs with a stretched shape (aspect ratio = 1.7) showed the lowest gas permeability, which is due to the better placement of the elliptical NPs in the Nafion microstructure, as also confirmed by small-angle X-ray scattering (SAXS) results (Figure S5). As shown in Figure S6, the membrane water uptake decreased with increasing NP size, similar to the trend previously discussed for pure PBI NPs. DSC was also used to characterize the state of the water in a nanocomposite membrane.<sup>20</sup> On the basis of the water swelling measurements and DSC results, the ratio of bound water to total membrane water was found to increase at least 50% in the presence of PBI NPs (Figure S6). In general, the percentage of bound water in the NP composite membranes decreased as the NP size increased, except for the Nafion/PBI-NP105 membrane, which had the highest degree of bound water (~76%).

To investigate further the capabilities of the fabricated PBI NPs and their contribution to the Nafion membrane microstructure, the proton conductivities of the related membranes were characterized. These results can be considered as indirect evidence of the effect of NP aspect ratio on the properties of the resultant membrane. It is clear that NPs larger than 70 nm could not enter the ionic nanochannels of Nafion, but they did contribute in the formation of ion-rich regions, as confirmed by the creation of an ionomer peak in the SAXS data for the dried membranes (Figure S5). This morphological evolution inside the Nafion resulted in an enhancement of the membrane proton conductivity (Figure 3). As a control, it was shown that the presence of PBI via common blending with the Nafion polymer was unable to improve the ionic conductivity of the Nafion membrane. The membrane gas permeability followed the same trend as shown in the conductivity results.

Nafion/PBI-NP nanocomposite membranes had higher anhydrous conductivities in all ranges of temperature (25–

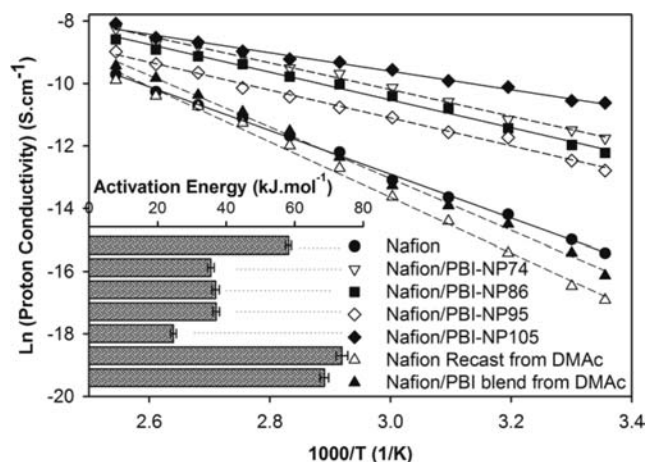


**Figure 3.** Arrhenius plots of the anhydrous proton conductivities of composite and pure membranes, an indicator of the main transport properties of the membranes that can control the electrochemical performance during fuel cell operation. Inset: activation energies for proton conduction in the membranes obtained from fits of the Arrhenius data.

120 °C) and lower activation energies ( $E_a$ ) compared with pure Nafion membranes (Figure 3 inset). These improvements in membrane performance may be due to the creation of new proton transfer pathways. It seems that elliptical NPs (e.g., 105 nm PBI NPs) are more desirable for forming composites with Nafion microstructures, a result that agrees with our prior research on hydroxyapatite NPs.<sup>21</sup> The conductivity results clearly confirmed that the shape of the NPs has a great influence on the performance of the resultant membranes. Nafion/PBI-NP105 composite membranes, relative to pure Nafion membranes, showed an improvement in conductivity of ~4 orders of magnitude at low temperatures and ~2 orders of magnitude at elevated temperatures under anhydrous conditions. The presence of fixed water and ion-rich nanochannels at the Nafion–PBI interface can result in higher conductivities at lower relative humidity (RH) and higher temperatures. Moreover, the benzimidazole groups of PBI can act as an ionic liquid (IL), supplying ion conduction under water-free conditions.

The fuel cell performance of the nanocomposite membranes was evaluated with a laboratory-made single-cell PEMFC under nonhumidified conditions at 120 °C (Figure 4). Membrane kinetic parameters can be derived by curve fitting of cell potential ( $E$ ) versus current density ( $I$ ) data.<sup>22</sup> We found that the membrane ohmic resistance ( $R$ ) was reduced significantly in the presence of PBI NPs, from 2.31  $\Omega$  cm<sup>-2</sup> for pure Nafion to 0.64  $\Omega$  cm<sup>-2</sup> for Nafion/PBI-NP. This observation revealed that the addition of PBI NPs decreases the ohmic resistance of the fuel cell, which indicates the existence of high proton conductance through the ion exchange membrane. The reduction in membrane resistance is highly desirable for fuel cell applications and results from the proton conduction properties and IL nature of PBI. Because of the enhanced proton/fuel gas permselectivity of nanocomposites, the open-circuit voltage under operating conditions increased significantly from 748 to 909 mV, which is among the highest reported values for anhydrous fuel cell operation.<sup>23</sup>

Under these low-humidity, high-temperature conditions, the maximum power output ( $P_{max}$ ) for a Nafion/PBI-NP105 membrane was ~287 mW cm<sup>-2</sup>, which is ~3 times higher

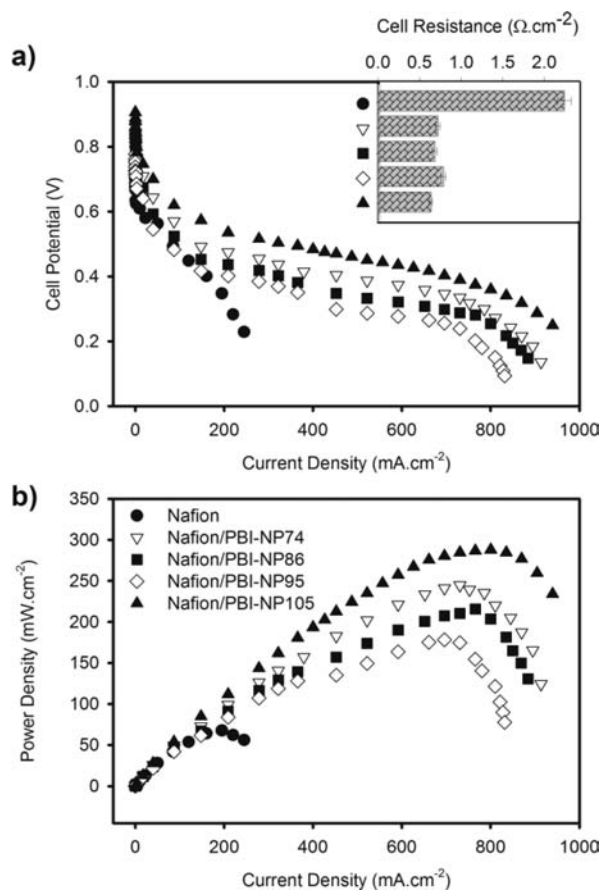


**Figure 4.** (a) Polarization curves and (b) power–current curves for nonhumidified hydrogen–oxygen single-cell PEMFCs consisting of pure Nafion and Nafion/PBI-NP composite membranes. The composite membranes used various PBI NP types at 2.0 wt %. The inset in (a) shows the membrane ohmic resistance.

than  $P_{\max}$  for a pure Nafion membrane of the same thickness ( $68 \text{ mW cm}^{-2}$ ). The results of durability performance tests (results not shown) also confirmed the stability of PBI NPs after more than 200 h of continuous operation in a PEMFC. The fuel cell performance degraded by <12%, whereas the performance degradation for a pure Nafion membrane was ~20%.

In conclusion, here we have presented a new microfluidic-based system to tune the parameters of PBI NPs. When applied to Nafion membranes to create composite fuel cell membranes, these NPs improved the fuel cell performance significantly. We have shown that the ability to tune the PBI NP properties results in the ability to tune the performance of the resultant fuel cell membranes. Of special note, we discovered that the NP aspect ratio is extremely important for making a functional ion exchange nanocomposite. This method for PBI NP tuning can be extended to the synthesis of other types of tailored (size/composition/shape) polymeric NPs, especially from liquid-crystalline polymers, and has the possibility to impact a wide range of applications.

## ■ ASSOCIATED CONTENT

### 📄 Supporting Information

Experimental details and supporting results. This material is available free of charge via the Internet at <http://pubs.acs.org>.

## ■ AUTHOR INFORMATION

### Corresponding Author

mahdi.hasani@gmail.com; philippe.renaud@epfl.ch

### Notes

The authors declare no competing financial interest.

## ■ ACKNOWLEDGMENTS

The authors thank Mr. H. Van Lintel and Mr. M. Taghipoor of LMIS4-EPFL for their helpful technical assistance and Dr. Carrie E. Brubaker and Prof. J. A. Hubbell (LMRP-IBI-EPFL) and Prof. Francesco Stellacci (SUNMIL-IMX-EPFL) for helpful discussions and critical reading of the manuscript. M.M.H.-S., F.S.M., and E.D. thank Prof. H. Modarres (Chemical Engineering, AUT) and Prof. N. Mohammadi (Polymer Engineering, AUT) for helpful fundamental discussions. This research was performed in the framework of the Biologically Inspired Developing Advanced Research (BIDAR) Group.

## ■ REFERENCES

- (1) Balazs, A. C.; Emrick, T.; Russell, T. P. *Science* **2006**, *314*, 1107.
- (2) Ikkala, O.; ten Brinke, G. *Science* **2002**, *295*, 2407.
- (3) D'Addio, S. M.; Prud'homme, R. K. *Adv. Drug Delivery Rev.* **2011**, *63*, 417.
- (4) Rao, J. P.; Geckeler, K. E. *Prog. Polym. Sci.* **2011**, *36*, 887.
- (5) Wang, C.-W.; Sinton, D.; Moffitt, M. G. *J. Am. Chem. Soc.* **2011**, *133*, 18853.
- (6) Karnik, R.; Gu, F.; Basto, P.; Cannizzaro, C.; Dean, L.; Kyei-Manu, W.; Langer, R.; Farokhzad, O. C. *Nano Lett.* **2008**, *8*, 2906.
- (7) Majedi, F. S.; Hasani-Sadrabadi, M. M.; Emami, S. H.; Taghipoor, M.; Dashtimoghdam, E.; Bertsch, A.; Moaddel, H.; Renaud, P. *Chem. Commun.* **2012**, *48*, 7744.
- (8) Jahn, A.; Vreeland, W. N.; Gaitan, M.; Locascio, L. E. *J. Am. Chem. Soc.* **2004**, *126*, 2674.
- (9) Zhang, C.; Pansare, V. J.; Prud'homme, R. K.; Priestley, R. D. *Soft Matter* **2012**, *8*, 86.
- (10) Li, Q.; Jensen, J. O.; Savinell, R. F.; Bjerrum, N. J. *Prog. Polym. Sci.* **2009**, *34*, 449.
- (11) Ainla, A.; Brandell, D. *Solid State Ionics* **2007**, *178*, 581.
- (12) Wycisk, R.; Chisholm, J.; Lee, J.; Lin, J.; Pintauro, P. N. *J. Power Sources* **2006**, *163*, 9.
- (13) Zhai, Y.; Zhang, H.; Zhang, Y.; Xing, D. *J. Power Sources* **2007**, *169*, 259.
- (14) Majedi, F. S.; Hasani-Sadrabadi, M. M.; Dashtimoghdam, E.; Haghghi, A. H.; Bertsch, A.; Moaddel, H.; Renaud, P. *Phys. Status Solidi RRL* **2012**, *6*, 318.
- (15) Shogbon, C. B.; Brousseau, J.-L.; Zhang, H.; Benicewicz, B. C.; Akpalu, Y. A. *Macromolecules* **2006**, *39*, 9409.
- (16) Zhang, C.; Guo, Y.; Priestley, R. D. *Macromolecules* **2011**, *44*, 4001.
- (17) Asensio, J. A.; Sanchez, E. M.; Gomez-Romero, P. *Chem. Soc. Rev.* **2010**, *39*, 3210.
- (18) Ma, C.-H.; Yu, T. L.; Lin, H.-L.; Huang, Y.-T.; Chen, Y.-L.; Jeng, U. S.; Lai, Y.-H.; Sun, Y.-S. *Polymer* **2009**, *50*, 1764.
- (19) Yampolskii, Y. *Macromolecules* **2012**, *45*, 3298.
- (20) Choi, B. G.; Hong, J.; Park, Y. C.; Jung, D. H.; Hong, W. H.; Hammond, P. T.; Park, H. *ACS Nano* **2011**, *5*, 5167.
- (21) Hasani-Sadrabadi, M. M.; Mokarram, N.; Azami, M.; Dashtimoghdam, E.; Majedi, F. S.; Jacob, K. I. *Polymer* **2011**, *52*, 1286.
- (22) Adjemian, K. T.; Dominey, R.; Krishnan, L.; Ota, H.; Majsztzik, P.; Zhang, T.; Mann, J.; Kirby, B.; Gatto, L.; Velo-Simpson, M.; Leahy, J.; Srinivasan, S.; Benziger, J. B.; Bocarsly, A. B. *Chem. Mater.* **2006**, *18*, 2238.
- (23) Zhang, H.; Shen, P. K. *Chem. Soc. Rev.* **2012**, *41*, 2382.